



# Evaporation from an open cylinder

G.D. McBain\*, H. Suehrcke, J.A. Harris

*School of Engineering, James Cook University, Townsville, QLD 4811, Australia*

Received 20 April 1999; received in revised form 9 September 1999

## Abstract

The rate of evaporation from the wetted floor of a tube open at the top to a relatively dry environment is investigated analytically, numerically and experimentally for the case of a light vapour. Though buoyancy forces ensure that the heavier external gas is always in motion, it is found that inside the tube both stagnation (diffusion-dominated evaporation) and convection are possible. In contrast to previous studies, axisymmetry of the postcritical flow is not assumed, leading to a reduction in the predicted critical Rayleigh number by a factor of 5 and much better agreement with experiment. © 2000 Elsevier Science Ltd. All rights reserved.

*Keywords:* Natural convection; Stability; Stefan diffusion tube; Evaporation; Interfacial velocity; Three-dimensional flow

## 1. Introduction

It is well known that in closed containers heated from below, unstable stratification with no flow is possible below a certain critical value of the vertical density gradient [1]. If this value is exceeded, convective motion is initiated, leading to higher heat transfer rates.

The common case of a container heated from below with an open top is less clear, since some convective motion always occurs (see Section 2.1). The relative thermal conductivity of the container walls and the size and shape of the surroundings both influence the flow pattern in the container and, hence, the heat transfer rate. An example of this is the open thermosyphon, for which Weiss and Shai [2] have recently shown that under certain conditions the cold fluid from the ambient does not penetrate into the cylinder;

i.e. a closed convective cell is possible. This is in contrast with the earlier assumption [3,4] that the fluid heated in the cylinder is discharged from the open end and continuously replaced by cold ambient fluid.

In this paper, the onset of mass transfer-driven natural convection in an open cylinder partially filled with water is studied using a combination of experiment, analysis and numerical modelling. The cylinder is placed at the base of a relatively large isothermal cube so that the ambient conditions are determinate. The positive buoyancy of the water vapour in air drives a convective flow in the cylinder and ambient which is the subject of this investigation.

One application of this problem is to the estimation of the error caused by evaporation in rain gauges [5]. Since the walls of the cylinder are impermeable and the mass fraction differences are small, this problem is analogous to an open cylinder with perfectly adiabatic walls that is heated from below.

### 1.1. Outline of the problem

Consider a solid cylindrical wall standing in the

\* Corresponding author. Tel.: +61-7-47-81-55-12; fax: +61-7-47-81-46-60.

*E-mail address:* megdm@jcu.edu.au (G.D. McBain).

### Nomenclature

$D_{AB}$	binary diffusivity
$\mathbf{g}$	gravitational acceleration
$Gr$	Grashof number, $g\zeta(m_{*1} - m_{*0})R_*^3/\nu^2$
$H$	reduced cylinder height, $H_*/R_*$
$\hat{\mathbf{k}}$	unit vertical vector
$L$	reduced enclosure size, $L_*/R_*$
$M$	evaporation rate
$m$	reduced vapour mass fraction, $(m_* - m_{*0})/(m_{*1} - m_{*0})$
$\hat{\mathbf{n}}$	unit normal vector
$Nu$	Nusselt number, thermal analogue of $Sh$
$p$	reduced pressure, $(p_* + \rho g z_*)R_*^2/\rho\nu^2$
$Pr$	Prandtl number, thermal analogue of $Sc$
$R$	cylinder radius or (Section 3.1) mass transfer resistance
$r$	reduced cylindrical radial coordinate, $r_*/R_*$
$Ra$	Rayleigh number, or $Gr Sc$ or $Gr Pr$
$Sc$	Schmidt number, $\nu/D_{AB}$
$Sh$	Sherwood number, $MH/\rho D_{AB} R_* \pi \Phi$
$T$	reduced cylinder wall thickness, $T_*/R_*$
$t$	reduced time, $t_*\nu/R_*^2$
$\mathbf{u}$	reduced velocity, $\mathbf{u}_*R_*/\nu$

$w$	reduced vertical component of velocity, $\hat{\mathbf{k}} \cdot \mathbf{u}$
$z$	reduced vertical coordinate, $z_*/R_*$

### Greek symbols

$\zeta$	vapour mass fraction coefficient of volumetric expansion
$\theta$	longitude
$\nu$	kinematic viscosity
$\xi$	eigenvalue of Ostroumov's solution, Eq. (22)
$\rho$	mixture density
$\Phi$	mass transfer rate factor, $\ln[(1 - m_{*0})/(1 - m_{*1})]$

### Subscripts

*	dimensional
0	at the base of the cube
1	at the base of the cylinder
1D	Stefan diffusion tube
c	critical
cyl	space inside cylinder
ext	space outside cylinder

centre of the floor of a cube filled with a nonreacting gas (see Fig. 1). The floor of the cylinder is a source of vapour and the floor of the cube is a sink. The other surfaces are impermeable to the vapour. All surfaces are impermeable to the gas and nonslip.

For example, the gas could be air, the walls glass or acrylic, the bottom of the cylinder wet with water and the rest of the base of the cube wet with a brine. The vapour will be saturated over the cylinder base. By varying the salt or its concentration, a wide range of sink relative humidities is possible [6].

If the system is isothermal, the only causes of motion are the interfacial velocity at the vapour source and sink and buoyancy forces due to the dependence of the mixture density on the vapour mass fraction. If, then, the Boussinesq approximation is made, the conservation equations for the gas–vapour mixture are [7]:

$$\nabla \cdot \mathbf{u} = 0 \quad (1)$$

$$\frac{\partial \mathbf{u}}{\partial t} + \mathbf{u} \cdot \nabla \mathbf{u} = -\nabla p + Gr m \hat{\mathbf{k}} + \nabla^2 \mathbf{u} \quad (2)$$

$$\frac{\partial m}{\partial t} + \mathbf{u} \cdot \nabla m = \frac{1}{Sc} \nabla^2 m \quad (3)$$

subject to

$$\mathbf{u} = \frac{e^\Phi - 1}{[(e^\Phi - 1)m - e^\Phi] Sc} \nabla m, \quad (4)$$

and

$$m_1 = 1, m_0 = 0 \quad (5)$$

at the source and sink and

$$\mathbf{u} = \mathbf{0}, \quad (6)$$

$$\hat{\mathbf{n}} \cdot \nabla m = 0 \quad (7)$$

on the solid surfaces. The interfacial velocity boundary condition (4) arises from the conservation of mass and the impermeability of the surfaces to the gas — see Rosenberger and Müller [8] or McBain [9] for a derivation. In the air–water vapour example, it is a consequence of the near insolubility of air in water.

### 1.2. Evaporation rate

By Eq. (4), the evaporation rate can be calculated either from the interfacial velocity or from the gradient of the mass fraction field:

$$M = \rho v R_* \int_0^1 \int_0^{2\pi} r w|_{z=0} d\theta dr$$

$$= \rho v R_* \frac{1 - e^\Phi}{Sc} \int_0^1 \int_0^{2\pi} r \frac{\partial m}{\partial z}|_{z=0} d\theta dr. \tag{8}$$

If  $m = 0$  is applied at the cylinder mouth, the no-slip condition (6) at the cylinder wall is neglected; and if  $Gr = 0$ , the system reduces to a Stefan diffusion tube [10]. Thus:

$$\mathbf{u}_{1D} = \frac{\Phi}{H Sc} \hat{\mathbf{k}}, \tag{9}$$

$$\nabla p_{1D} = \mathbf{0}, \tag{10}$$

$$m_{1D} = \frac{\exp(\Phi z/H) - \exp(\Phi)}{1 - \exp(\Phi)}, \tag{11}$$

from which the constant-density equivalent of Stefan's Law is obtained:

$$M_{1D} = \frac{\rho D_{AB} R_* \pi \Phi}{H}. \tag{12}$$

This is used as a reference evaporation rate to define the Sherwood number,  $Sh$  [11,12].

### 1.3. The low mass transfer rate limit

A rational approximation to the system at low mass transfer rates is formally obtained by letting  $\Phi$  tend to zero and neglecting terms  $o(1)$ . In this low mass transfer rate limit, Eq. (4) is replaced by Eq. (6) and the reduced evaporation rate is given by the limiting form of Eq. (8):

$$Sh \sim \frac{-H}{\pi} \int_0^1 \int_0^{2\pi} r \frac{\partial m}{\partial z}|_{z=0} d\theta dr \quad (\Phi \rightarrow 0). \tag{13}$$

This small  $\Phi$  approximation is used hereafter.

Note that Eq. (13) is not quite the same as the equation recommended in elementary mass transfer textbooks [13]. The right-hand side is the same, and is also formally identical to the usual expression for the Nusselt number [13], but the left-hand side uses for the driving force not a mass fraction difference, but  $\Phi$ . The present definition obviates the need for a 'mass transfer correction factor', such as used by Bird et al. [14], Spalding [15] and Suehrcke and McBain [16], when comparing results at high and low mass transfer rates.

It is interesting to note that with the present definitions, the one-dimensional Stefan diffusion tube problem (Section 1.2) can be solved by neglecting the interfacial velocity; the answer obtained,  $Sh = 1$ , will be correct at all values of  $\Phi$ .

## 2. General considerations

### 2.1. The parameter space

Apart from whatever initial conditions may be prescribed, and using the small  $\Phi$  approximation developed in Section 1.3, the problem depends on five dimensionless parameters:  $H$ ,  $L$ ,  $T$ ,  $Sc$  and  $Gr$ . The first four of these are necessarily nonnegative.

The Grashof number and the vapour mass fraction coefficient of volumetric expansion,  $\zeta$ , have the same sign: positive if admixture of the vapour decreases the density of the mixture. Given the above mass transfer boundary conditions, neither sign leads to a trivial

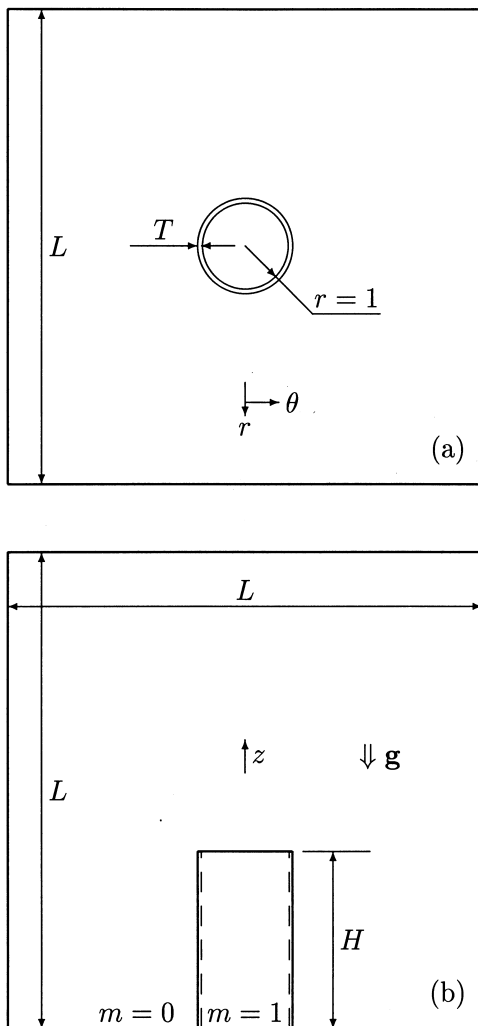


Fig. 1. Geometry: (a) plan and (b) elevation. The radial vector is shown in (a) in the  $\theta = 0$  position.

problem; i.e. one with  $\mathbf{u} \equiv \mathbf{0}$ . This can be seen by taking the curl of the momentum equation (2) and setting the velocity to zero:

$$\mathbf{0} = -Gr \hat{\mathbf{k}} \times \nabla m, \quad (14)$$

so that  $Gr \neq 0$  implies  $m = m(z)$ , only, which is impossible for solutions of Eqs. (3) and (5) in the present geometry [17]. This is to be contrasted with the situation for infinite horizontal layers [18] or closed cylinders [19,20], where there exist hydrostatic solutions for all  $Gr$ .

If the cylinder is tall enough, the presence of the solid walls may be sufficient to damp out any internal motion. This is suggested by the numerical solutions of Goldstein and Lau [21] (cited in Section 2.2) or consideration of the  $H \rightarrow \infty$  limit [22,23]. For  $Gr > 0$ , the fluid is then unstably stratified. It is these configurations, allowing the possibility of either stagnation or convective instability in the cylinder, that are of greatest interest in the present study.

Since the most common gas–vapour pair is air–water vapour, and this has  $\zeta > 0$ , we consider only positive Grashof numbers and take  $Sc = 0.614$ . At temperatures below 50°C, water vapour makes up less than 10% of air by mass, so that  $\Phi < 10^{-1}$  and the approximation for small  $\Phi$ , developed in Section 1.3, is useful. The values involved in the present experiments are an order of magnitude smaller still (see Section 4.2).

The cube is only introduced to render the problem determinate; the focus is the behaviour in the cylinder. Values of  $L$  large enough for it to have no effect on  $Sh$  are of particular interest, since then, presumably, the cube could be replaced by any other shaped boundary lying outside it. This is not to say that the fluid far from the cylinder is quiescent (see the photographs cited in Section 2.2), only that its motion has a negligible influence on the evaporation rate. The cylinder wall thickness,  $T$ , is usually small ( $\ll 1$ ).

## 2.2. Regimes

The photographs made by Torrance et al. [24] of the flow in the thermal analogue of the special case  $H = 0$ , localized heating of a disk in the centre of the floor of an enclosure, show that for  $Gr < 10^4$  (at  $T = 0.7$ ,  $Sc = 0.7$ ,  $\Phi = 0$  and  $L$ , based on height for noncubical enclosures, of 15.2), the flow is essentially axisymmetric except near the enclosure walls. The basic structure is a central plume through a horizontal vortex ring. Comparable images of isolated plates have been recorded [25].

A similar structure occurs in Goldstein and Lau's [21] two-dimensional numerical solutions. They also investigated the effect of vertical walls around the

plate (finite  $H$ ), including experiments on open square cylinders. These measurements showed that for small  $Gr$  increasing  $H$  significantly reduced the mass transfer rates, as the walls block the flow to the plate, although the effect is reduced at higher  $Gr$ . Their numerical solution at  $Sc = 0.7$ ,  $H = 2$  and  $Gr = 1.1 \times 10^3$  (the length scale being the plate area to perimeter ratio) shows stagnant fluid and diffusion-dominated transfer in the walled space, indicating unstable stratification. It might be suggested that the lack of spatial resolution and the restrictions placed on the flow (steadiness, planarity and possibly symmetry about the vertical midplane, although the paper is unclear on the point) in their numerical solutions prevented gravitational instabilities and so were responsible for the lack of agreement with their experiments. The numerical Sherwood numbers do not show the transition at  $Gr \approx 10^2$  of their measurements. It is known [23] that for very tall rectangles of unstably stratified fluid, the most easily excited plane disturbances (excluding the even more likely three-dimensional modes [26]) are antisymmetric. The symmetry at the onset of convective evaporation in a circular cylinder will be shown in Section 4 to have a clear parallel with this problem.

At higher Rayleigh numbers ( $10^5$ – $10^8$ , for  $3.5 < Pr < 1650$ ) small walls ( $H = 0.18$ ) around a heated circular plate actually increase the heat transfer rate, while taller walls ( $H > 0.8$ ) seem to have little effect [27]. This latter finding is consistent with the trend for enclosures heated from below: at high enough,  $Ra$ ,  $Nu$  becomes independent of the aspect ratio [28,29].

For very large  $H$ , the difference between open and closed cylinders diminishes. This means the asymptotic results of Ostroumov [22], Yih [23] and Verhoeven [30] become available. In particular, it is known that for  $Gr < 67.8H Sc^{-1}$ , the fluid is stable with respect to all disturbances, and for higher  $Gr$ , the initial growth of small disturbances is monotonic in time, rather than oscillatory, and that the symmetry of the preferred mode is diametral antisymmetry rather than axisymmetry.

As indicated in Section 2.1, the principal question addressed in this study is the effect of  $Gr$  and  $H$  on  $Sh$ , for  $Sc = 0.614$ , large  $L$  and small  $T$  and  $\Phi$ . In particular, whether the cylinder walls can render the internal fluid stagnant, and, if so, under what conditions gravitational instability can occur. In Section 3, the possibility of stagnation is assumed, and the resulting evaporation predicted. In Section 4, the experimental method is described and evaporation measurements reported for  $H = 4$ . The results, which indicate a convective transition, are supported by full numerical solutions of Eqs. (1)–(3). The critical density difference is

estimated and the structure of the supercritical flow examined.

### 3. The stagnant cylinder

#### 3.1. An approximate analytical treatment

For  $Gr = \Phi = 0$  and  $t \rightarrow \infty$ , the equations reduce to  $\mathbf{u} = \nabla p = \mathbf{0}$  and

$$\nabla^2 m = 0, \tag{15}$$

with Eqs. (5) and (7) as boundary conditions.

It is not possible to obtain an exact solution of Eq. (15) in this geometry, but the mass transfer between the floor of the cylinder and the floor of the cube can be modelled as a path consisting of two serial resistances,  $R_{cyl}$  and  $R_{ext}$ .

Assuming one-dimensional diffusion in the cylinder, its resistance is  $R_{cyl} = 1$ .

The external resistance is more complicated, but if the cube walls are distant, the cylinder is tall and its walls thin ( $L \gg H \gg 1 \gg T$ ), the mass transfer will resemble that between a point source at  $r = 0, z = H$  and a zero wall at  $z = 0$ . This is identical to the mass transfer between a point source at  $r = 0, z = H$  and a point sink of equal strength at  $r = 0, z = -H$ . The solution for  $m$  in this simplified problem is [31]:

$$m = \frac{Sh}{4H} \left\{ [r^2 + (z - H)^2]^{-1/2} - [r^2 + (z + H)^2]^{-1/2} \right\}. \tag{16}$$

To construct an appropriate resistance for the exterior, a mass fraction difference is required ( $m$  is singular at the point source). To this end, the mean value of  $m$  is taken over the disk where the mouth of the cylinder would be,

$$\begin{aligned} \bar{m} &= \frac{1}{\pi} \int_0^1 2\pi r m|_{z=H} dr \\ &= \frac{Sh}{2H} \left[ 1 + 2H - (1 + 4H^2)^{1/2} \right]. \end{aligned} \tag{17}$$

The external resistance is  $R_{ext} = \bar{m}/Sh$ , so that the evaporation rate is

$$Sh = \frac{1}{R_{cyl} + R_{ext}} = \frac{2H}{1 + 4H - (1 + 4H^2)^{1/2}}. \tag{18}$$

For the large values of  $H$  consistent with the derivation, this is approximately

$$\frac{H}{\frac{1}{2} + H}. \tag{19}$$

#### 3.2. Verification

To test Eq. (19), numerical solutions of Eq. (15) were generated with the fluid dynamics analysis package FIDAP [32]. So as to reduce the dimensionality of the problem, the cubical enclosure was replaced with a coaxial cylinder of height and diameter  $L$ . For values of  $L$  large enough not to affect  $Sh$ , the enclosure shape should be irrelevant. The results of a series of runs showing the diminishing effect of increasing enclosure size are plotted in Fig. 2. The effect of cylinder aspect ratio,  $H$ , is given in Fig. 3, where  $L = 10H$  is used to give ‘large’ enclosure results. Eqs. (18) and (19) are seen to perform well at the higher values of  $H$ , as expected, but the fit can be much improved by adjusting the constant in Eq. (19) to give:

$$Sh = \frac{H}{0.594 + H} \quad (Gr = 0). \tag{20}$$

This semiempirical formula fits the FIDAP data of Fig. 3 to better than 0.3% for  $H > 1$ . A comparison with experimental and numerical results at  $H = 4$  is given in Section 4.

### 4. Convective evaporation

There have been a number of studies on evaporation from open cylindrical containers under isothermal con-

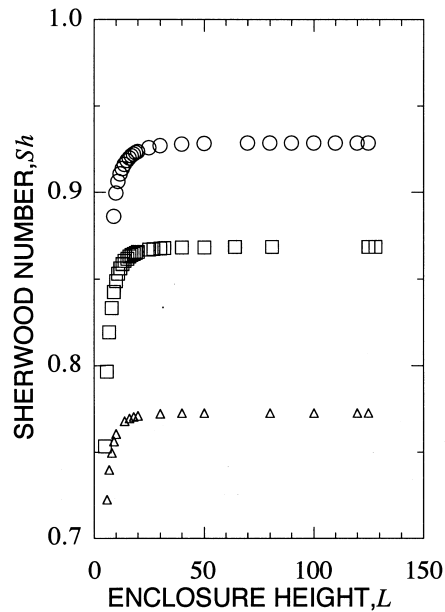


Fig. 2. The diminishing effect of enclosure size on evaporation rate. FIDAP solutions for  $T = 0.05$  and  $Gr = 0$ , for enclosures of circular platform; height and diameter equal to  $L$ . Legend:  $\circ H = 8$ ;  $\square H = 4$ ;  $\triangle H = 2$ .

ditions [33–38]. The numerical study of Sparrow et al. [33] considered  $2 \leq H \leq 10$  for  $Gr = 10^3$  and  $10^4$ , whereas that of Nunez and Sparrow [35] covered  $0.7 \leq H \leq 6$  for  $Gr = 1917$ . Sparrow and Nunez [36] presented measurements for  $0.4 \leq H \leq 5.7$  with  $Gr = 1708$  and  $2000$ . Suehrcke and Harris [37] presented numerical and experimental data for  $H = 3.5$  over the range  $1000 \leq Gr \leq 30,000$ . They demonstrated that various axisymmetric steady-state flow modes were possible and that the flow was convectively stable (with respect to axisymmetric disturbances) for  $Gr \leq 3000$ .

Without exception, the numerical simulations reported in these studies assumed that the flow is axisymmetric and so precluded the possibility of other modes, such as the diametrically antisymmetric mode mentioned in Section 2.2. In this section, a combination of experimental measurements and three-dimensional numerical simulations are used to demonstrate that for isothermal evaporation at  $H = 4$ , the most unstable flow mode is diametric antisymmetry.

#### 4.1. Predicting the onset of convection

The onset of convection in closed vertical cylinders can be predicted by linear stability analysis [19,20,39]. This is much more difficult for the open case, however, since (a) there is no truly stagnant state and (b) the boundary conditions at the mouth cannot be simply

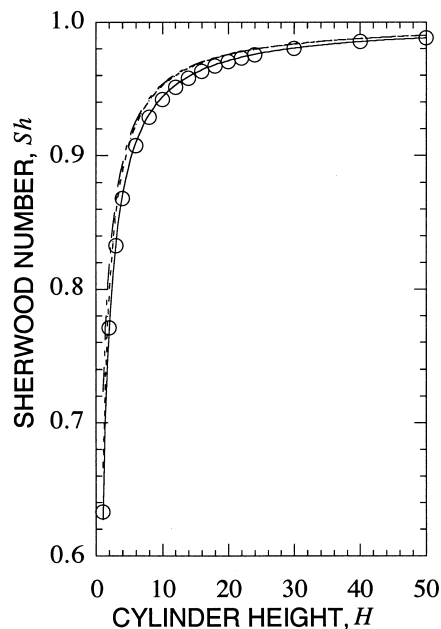


Fig. 3. Purely diffusive evaporation from an open cylinder in a large enclosure. Legend: - - - Eq. (18); - · - Eq. (19); — Eq. (20); ○ FIDAP results (axisymmetric, cylindrical enclosure of height and diameter  $10H$ ,  $T = 0.05$ ).

specified. Nevertheless, an approximate answer can be obtained by neglecting (a) and treating (b) by imposing at the mouth a stress-free condition on the velocity and on the mass fraction the approximate pure-diffusion value,  $m = H/(0.594 + H)$ , obtained in Section 3. By symmetry, then, this would give the same critical vertical density gradient for an open cylinder of height  $H$  as for a closed cylinder of height  $2H$ . The criterion for closed cylinders is given as a critical value of  $(Ra H^{-1})$ , which is a weak function of  $H$  for large  $H$  [30].

Thus, the critical Grashof number for convective instability is predicted to be

$$Gr_c \approx \frac{0.594 + H}{Sc} (Ra_c H^{-1})|_{(2H)}. \quad (21)$$

Applying Eq. (21) to the experimental arrangement ( $Sc = 0.614$ ,  $H = 4$ ), and obtaining  $(Ra_c H^{-1})$  by interpolating Verhoeven's table [30], gives  $Gr_c \approx 550$ . This figure and the preceding analysis are tentative; a description of experiments and numerical solutions performed to determine the criterion more accurately follows.

#### 4.2. Experiments

The experimental apparatus was essentially the same as that used in the earlier study [37]. Water was pumped from a variable thermostatic bath through copper pipes embedded in each of the polystyrene-clad 20 mm thick aluminium sides of the cube ( $L_* = 441 \pm 2$  mm; uncertainties are quoted at a 95% confidence level throughout). The cylinder ( $R_* = 17.45$  mm, with standard deviation 0.07 mm,  $T = 0.113 \pm 0.004$ , total depth  $72.99 \pm 0.02$  mm) holding  $2.0 \pm 0.1$  ml of distilled water had polycarbonate walls and a 5.7 mm thick aluminium base in direct contact with the floor of the cube and fitted with a platinum resistance temperature detector (PRTD). The remainder of the cube floor was bonded to the underside of a 3 mm thick perspex tray holding a saturated aqueous solution of sodium chloride. A combined hygrometer–PRTD was placed along one of the vertical edges and a third PRTD taped to one of the cube walls. All PRTDs were calibrated to 0.05 K. A pulley near the centre of one of the upper edges held a string which led outside the cube, enabling removal of the rubber lid of the cylinder an hour or so after installation and assembly of the cube and cylinder. This allowed control of the initial conditions, though the transient response was of no concern in the present study.

The measured quantities were: the dimensions and mass of the dry cylinder; the duration of each run; the mass of the cylinder before and after the run (from which both  $M$  and  $H_*$  were determined); and the three PRTD temperatures. The relative humidity of the cube

Table 1  
Reduced experimental results, including 95% confidence intervals

$\phi \times 10^3$	$Gr$	$Sh$
$4.9 \pm 0.2$	$610 \pm 30$	$0.87 \pm 0.06$
$11.8 \pm 0.9$	$1190 \pm 90$	$2.36 \pm 0.18$
$7.2 \pm 0.4$	$820 \pm 40$	$1.52 \pm 0.08$
$3.7 \pm 0.3$	$490 \pm 30$	$0.90 \pm 0.06$
$5.7 \pm 0.3$	$686 \pm 30$	$1.07 \pm 0.06$
$5.0 \pm 0.2$	$624 \pm 30$	$1.02 \pm 0.05$
$9.1 \pm 0.7$	$980 \pm 70$	$1.95 \pm 0.14$

air was also measured, but only to assess the steadiness of the system;  $m_{*1}$  and  $m_{*0}$  were calculated from the temperature readings and tabulated data for the vapour pressure over pure and salt water [40]. The reduced results are presented in Table 1 and Fig. 4.

The principal difficulties in the experiments were the geometry change from the fall in the level of the evaporating water, the change in the humidity over the brine due to dilution by condensate and the evaporative cooling of the source.

The accuracy of the scales (1 mg) allowed runs of relatively short duration (less than a day); the greatest

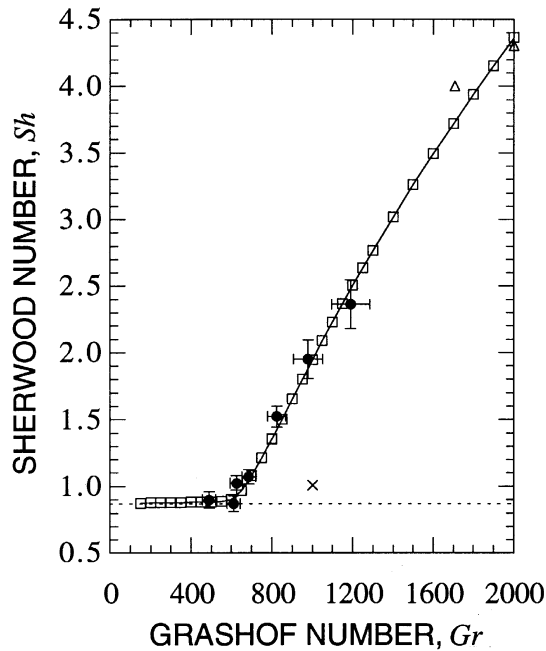


Fig. 4. Evaporation from an open cylinder into a heavy gas ( $H = 4$ ,  $L = 25.1$ ,  $T = 0.086$ ,  $Sc = 0.614$  and  $\Phi$  small). Legend: ● experimental (present study); △ experimental ([36], Figs. 3 and 4); -□- numerical (present study); --- diffusion limit, Eq. (20); × axisymmetric numerical result ([33], Fig. 2).

evaporative mass loss in any run was 442 mg, equivalent to a 0.6% increase in  $H$ . For all runs,  $H = 4.09 \pm 0.03$ .

The problem of variation in  $m_{*0}$  due to condensation in the brine was very small because of the low transfer rates, the large area of the sink and especially the shallowness of the brine layer. The tray was covered with excess solid salt, above which the maximum

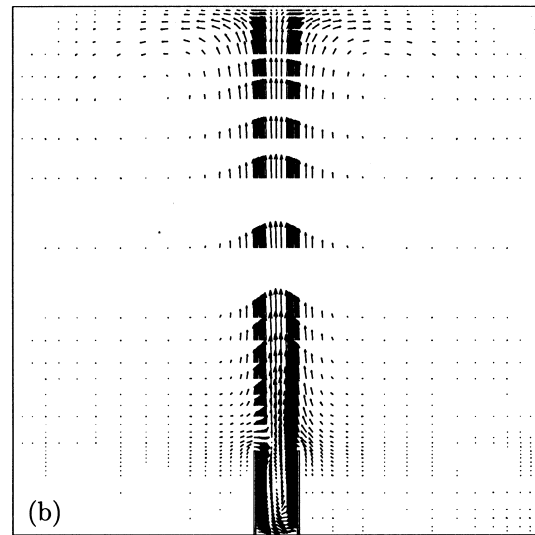
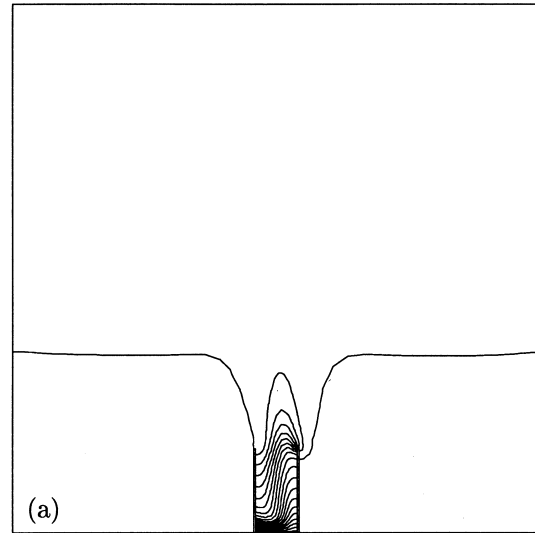


Fig. 5. A typical solution for convective evaporation from an open cylinder.  $H = 4$ ,  $L = 25.1$ ,  $T = 0.086$ ,  $Sc = 0.614$ ,  $Gr = 1300$ : (a)  $m$ , with contours at 0.025 (0.05) 0.975 and (b)  $u$ , with the maximum plotted vector having magnitude 21.24. The section shown,  $\theta = \pi/2, 3\pi/2$ , is a plane of symmetry.

liquid depth was about 2 mm. Assuming the solution to be saturated at the interface with the excess solid, the increase in the surface relative humidity should not have exceeded 0.02%, in spite of the low diffusivity of salt in water. It is estimated that the relative humidity at the sink was maintained to better than  $\pm 0.01$ .

The evaporation at the water surface is accompanied by a removal of heat of vaporization. This leads to a temperature depression, which is offset primarily by conduction through the water from the aluminium base. Ignoring the other compensatory effects, such as radiation, conduction from the cylinder walls and convective heat transfer from the air, the steady-state temperature depression can be conservatively estimated. This value (less than 0.1 K in all cases), the precision of the PRTDs and the spread in the three temperature measurements (up to 0.2 K) was used in estimating the uncertainty of the source temperature. Another problem with the evaporative cooling is that it produces a buoyancy effect counteracting the primary compositional one. Using the above estimate of the surface temperature depression, this was less than 4.4% in all cases, and so within in the confidence intervals quoted for  $Gr$ . Like the previous two errors, this one is systematic in that it increases with the evaporation rate. This is evident in the relative sizes of the error bars in Fig. 4. Achieving accurate results at higher Sherwood numbers would almost certainly require active control of the temperature, i.e. automatic heating of the cylinder base [37].

#### 4.3. Numerical solutions

The convective flow in the cylinder and cube shown in Fig. 1 was simulated using FIDAP [32]. This code solves general flow problems using the finite element method. The performance of FIDAP has been evaluated for various classical flows by Sohn [41] and examples of the application of FIDAP to natural convection mass transfer problems can be found in Refs. [7,37,38,42,43].

The steady-state form of the governing equations (1)–(3), subject to boundary conditions (5)–(7), were discretized and solved by the pressure projection segregated algorithm [44], the consistent finite element counterpart of the popular SIMPLER scheme [45] used in finite volume codes. Preconditioned conjugate residual and conjugate gradient squared iterative solvers were used for the solution of the symmetric and non-symmetric matrices, respectively, as recommended by Haroutunian et al. [44]. A sample solution is illustrated by a section through a plane of symmetry in Fig. 5.

The nonuniform three-dimensional finite element mesh was constructed of 27-node brick elements employing quadratic shape functions and a linear dis-

continuous pressure approximation. The 70,741 nodes and 10,596 elements were distributed so that they were concentrated near nonslip surfaces and inside the cylinder. The central region above the mouth of the cylinder contains some high aspect ratio elements; however, since the elements are aligned in the direction of flow and essentially no streamwise velocity gradient is expected in a buoyant plume [46] (see also Fig. 5), there should be little or no adverse effect on the solution. Simulations with this mesh typically required 40 iterations to reach the specified relative error tolerance of  $10^{-3}$ , taking approximately 6 h of CPU time on a single SGI R10000 processor.

A solution for  $Gr = 1000$  was obtained in the following manner. A stagnant flow field was used as the initial guess with the gravity vector tilted slightly to initiate a preferred flow direction. After a certain number of iterations the gravity vector was realigned with the  $z$ -axis and the solution allowed to reach steady-state. It was found that more than one steady-state solution was possible, depending on the initial gravity orientation. If  $\mathbf{g}$  was initially tilted in a plane parallel to either faces ( $\theta = 0$ ) or diagonals ( $\theta = \pi/4$ ) of the cube, the resulting steady-state solutions were observed to be symmetric about the same plane. In either case, and also when  $\mathbf{g}$  was initially tilted in the  $\theta = \pi/8$  plane, the flow field in the cylinder and the resulting evaporation rates were identical to four significant figures. These three cases are illustrated in Fig. 6, which shows

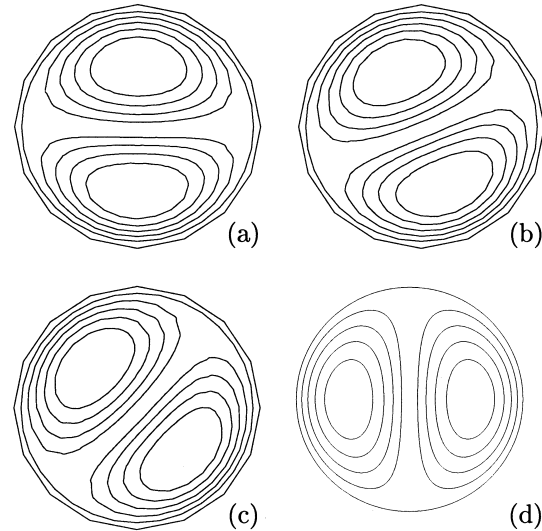


Fig. 6. Contours of  $w$  for convective evaporation from an open cylinder in the plane  $z = 2$ . Numerical results (parameters as in Fig. 7) obtained from an initial guess in which  $\mathbf{g}$  was tilted in the meridian plane: (a)  $\theta = 0$ , (b)  $\theta = \pi/8$  and (c)  $\theta = \pi/4$ . Compare (d) Ostroumov's asymptotic ( $H \rightarrow \infty$ ) solution, Eq. (22).

contours of  $w$  at the mid-height of the cylinder. The patterns are identical apart from the orientation, and are similar to the one-dimensional tall cylinder solution of Ostroumov [22],

$$w \propto \left[ \frac{J_1(\xi r)}{J_1(\xi)} - \frac{I_1(\xi r)}{I_1(\xi)} \right] \cos \theta, \quad \xi^4 = 67.8 \quad (22)$$

(the datum for  $\theta$  being arbitrary) which is also exhibited in Fig. 6 for comparison.

The solution for the case where the symmetry plane is parallel to the cube faces was used as a starting point for solutions at higher and lower Grashof numbers. A ramping procedure was used in

which the Grashof number was changed in a series of steps (typically 50 and 100) and the solution at the nearest Grashof number used as an initial guess. In all cases, the symmetry plane remained aligned with the cube faces. Subsequent results pertain to this series of runs.

Measured and predicted evaporation rates are compared in Fig. 4. The agreement is excellent over the range of  $Gr$  tested. Both sets of results tend to the diffusion limit ( $Sh = 0.871$ ) given by Eq. (20). These experimental data are not consistent with the axisymmetric model of the cylinder [33,37] which does not predict convective instability until  $Gr \approx 3000$  [37].

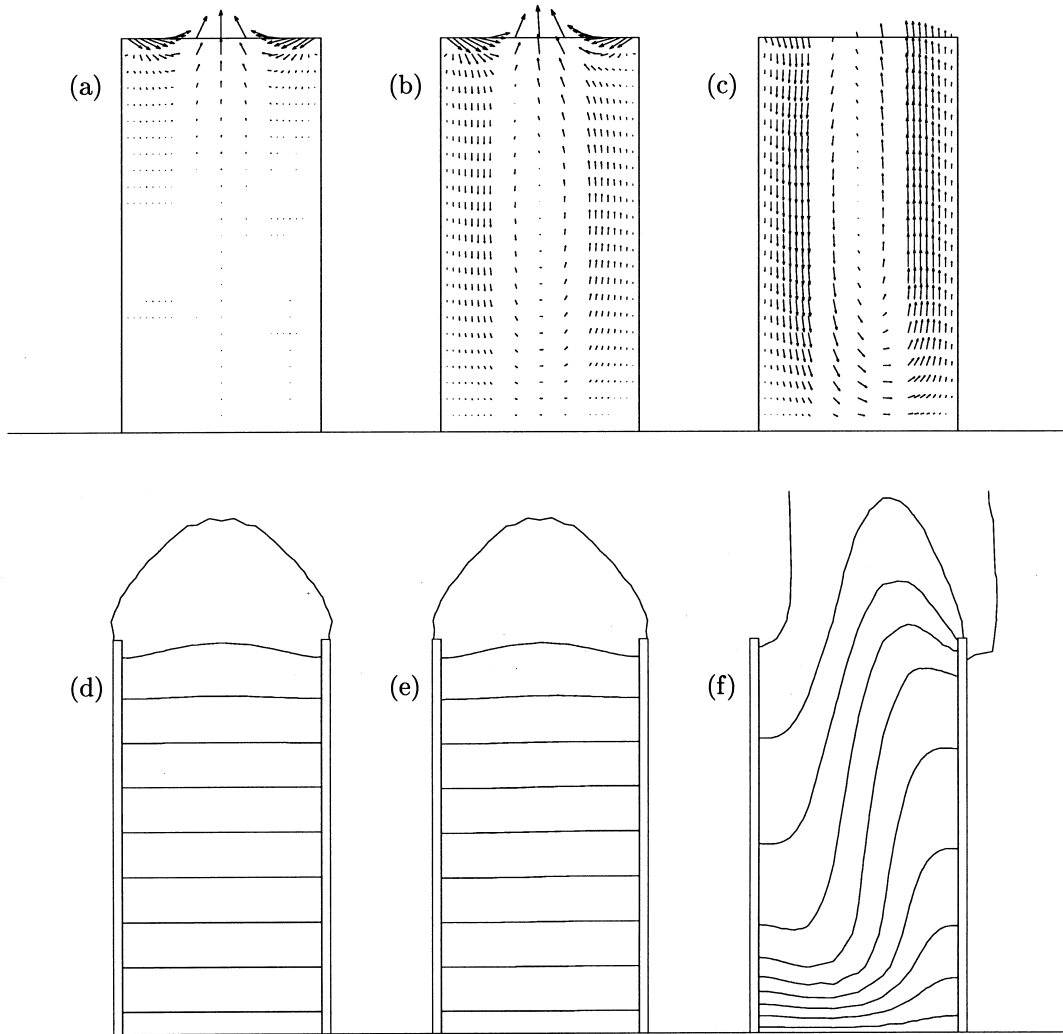


Fig. 7. Velocity (a–c) and mass fraction (d–f) solutions for evaporation from an open cylinder.  $H = 4$ ,  $L = 25.1$ ,  $T = 0.086$ ,  $Sc = 0.614$  and  $Gr = 350$  (a, d), 450 (b,e) and 1300 (c, f). The longest arrows plotted are (a) 0.3196, (b) 0.4323 and (c) 15.08. The contours (d–f) are at  $m = 0.05$  (0.1) 0.95.

Fig. 4 includes a point from this restricted model [33] which is clearly at odds with both the physical evidence and three-dimensional solutions.

The velocity and mass fraction fields in the  $\theta = 0, \pi$  plane for three Grashof numbers are shown in Fig. 7. For clarity, the velocity field is only plotted inside the cylinder, whereas the mass fraction contours extend into the exterior. These figures illustrate the progression from the essentially stagnant cylinder ( $Gr \leq 350$ , note that as stated in Section 2.1, there is a nonzero flow field for any finite value of  $Gr$ ) to convective flow ( $Gr = 450$ – $1300$ ). This mode only strictly exhibits the diametral antisymmetry of Eq. (22) in the linear limit; Fig. 7(b) is close to this, but the pattern becomes skewed by the increasing inertial forces at higher Grashof numbers as is evident in Fig. 7(c).

With any numerical model, it is important to assess the influence of mesh refinement and convergence tolerance [47]. Mesh refinement tests at  $Gr = 10^3$  indicated that the predicted evaporation rate changed by only 0.25 and 0.023% when the number of elements was increased from 3684 to 10,596, and from 10,596 to 21,948, respectively. Additionally, the computed evaporation rate typically changed by less than 0.05% when the relative convergence tolerance was decreased from  $10^{-3}$  to  $10^{-4}$ .

#### 4.4. Discussion

The discrepancy evident in Fig. 4 between the axisymmetric and three-dimensional models is very similar to the asymptotic ( $H \rightarrow \infty$ ) findings of Yih [23]: axisymmetric instability does not occur until  $Gr \geq 452H/Sc$  whereas the corresponding value for diametrically antisymmetric modes is  $Gr \geq 67.8H/Sc$ . Note that the figures 452 and 67.8 are in the same ratio as 3000 [37] and 450 (Fig. 7(b)).

Some simple smoke visualization tests were performed in an apparatus similar to the one described above but transparent. While it has not yet been possible to obtain publication quality images, the flow patterns were clearly visible to the naked eye and consistent with the three-dimensional numerical solutions.

The symmetry of the supercritical flow in the analogous thermal problem [3,4] may be different. Heat can be conducted to the fluid from all along the cylinder, favouring an axisymmetric flow up near the walls and down the axis. This axisymmetry has recently been experimentally demonstrated [2]. In closed cylinders with conducting walls, for which thermal contact with the cooled ceiling increases the (negative) vertical temperature gradient at the boundary, diametric antisymmetry is again the preferred mode for large  $H$  [48], as has been verified for  $H = 6$  [49].

## 5. Conclusion

While the velocity field cannot completely vanish in an open cylinder, the fluid inside can be rendered practically stagnant. Gravitational instability is also possible. This has been demonstrated for  $H = 4$ ; however, unlike in the case of closed cylinders, there is not a precise critical Rayleigh number, but rather a range over which the new flow mode emerges. For  $H = 4$  and  $Sc = 0.614$ , this is seen to be  $350 < Gr < 450$ , with the Sherwood number beginning to depart from the diffusion level at about  $Gr = 600$ .

The onset of convection is not necessarily axisymmetric. An incorrect assumption restricting the symmetry of the flow can result in a large overestimate of the critical vertical density gradient. For the present geometry, convection occurred at a Grashof number five times lower than predicted by previous axisymmetric analyses. Such an error leads to a gross underestimation of the evaporation rate for intermediate values of  $Gr$ .

## Acknowledgements

The authors would like to thank Professor Don Close for frequent helpful discussion. The rights to use FIDAP have been acquired by the School of Engineering under licence from Fluid Dynamics International. This work forms part of an Australian Research Council supported project.

## References

- [1] G.L. Raithby, K.G.T. Hollands, Natural convection, in: W.M. Rohsenow, J.P. Hartnett, E.N. Ganić (Eds.), *Handbook of Heat Transfer Fundamentals*, 2nd ed., McGraw-Hill, New York, 1985 (Chapter 6).
- [2] Y. Weiss, I. Shai, Typical heat transfer and flow regimes in the induced mixed convection phenomenon, in: J.S. Lee (Ed.), *Proceedings of the Eleventh International Heat Transfer Conference*, vol. 3, Taylor and Francis, Philadelphia, PA, 1998, pp. 281–286.
- [3] M.J. Lighthill, Theoretical considerations on free convection in tubes, *Quarterly Journal of Mechanics and Applied Mathematics* 6 (1953) 398–439.
- [4] S. Ostrach, P.R. Thornton, On the stagnation of natural-convection flows in closed-end tubes, *Transactions of the American Society of Mechanical Engineers* 80 (1958) 363–367.
- [5] R.C. Ward, *Principles of Hydrology*, McGraw-Hill, London, 1975, p. 32.
- [6] R.H. Stokes, R.A. Robinson, Standard solutions for humidity control at 25°C, *Industrial and Engineering Chemistry* 41 (1949) 2013.
- [7] G.D. McBain, J.A. Harris, The conduction–diffusion

- regime for convection in rectangular cavities filled with gas–vapour mixtures, in: J.S. Lee (Ed.), *Proceedings of the Eleventh International Heat Transfer Conference*, vol. 3, Taylor and Francis, Philadelphia, PA, 1998, pp. 379–384.
- [8] F. Rosenberger, G. Müller, Interfacial transport in crystal growth, a parametric comparison of convective effects, *Journal of Crystal Growth* 65 (1983) 91–104.
- [9] G.D. McBain, Heat and mass transfer across tall cavities filled with gas–vapour mixtures: the fully developed regime, *International Journal of Heat and Mass Transfer* 41 (1998) 1397–1403.
- [10] C.Y. Lee, C.R. Wilke, Measurements of gaseous diffusion co-efficients using the Stefan cell, *Industrial and Engineering Chemistry* 46 (1954) 2381–2387.
- [11] B.S. Jhaveri, F. Rosenberger, Expansive convection in vapor transport across horizontal rectangular enclosures, *Journal of Crystal Growth* 57 (1982) 57–64.
- [12] P. Ranganathan, R. Viskanta, Natural convection in a square cavity due to combined driving forces, *Numerical Heat Transfer* 14 (1988) 35–39.
- [13] F.P. Incropera, D.P. DeWitt, *Fundamentals of Heat and Mass Transfer*, 3rd ed., Wiley, New York, 1979, pp. 347–348.
- [14] R.B. Bird, W.E. Stewart, E.N. Lightfoot, *Transport Phenomena*, Wiley, New York, 1960, p. 663.
- [15] D.B. Spalding, *Convective Mass Transfer*, Edward Arnold, London, 1963, pp. 143–162.
- [16] H. Suehrcke, G.D. McBain, The effect of humidity on the heat and mass transfer across narrow vertical air spaces, in: J.S. Lee (Ed.), *Proceedings of the Eleventh International Heat Transfer Conference*, vol. 5, Taylor and Francis, Philadelphia, PA, 1998, pp. 157–162.
- [17] G.Z. Gershuni, E.M. Zhukhovitskii, *Convective Stability of Incompressible Fluids*, D. Louvish (Trans.), Keter, Jerusalem, 1976, p. 6.
- [18] A. Pellew, R.V. Southwell, On maintained convective motion in a fluid heated from below, *Royal Society of London: Proceedings Series A (Mathematical and Physical Sciences)* 176 (1940) 312–343.
- [19] G.S. Charlson, R.L. Sani, Thermoconvective instability in a bounded cylindrical fluid layer, *International Journal of Heat and Mass Transfer* 13 (1970) 1479–1496.
- [20] G.S. Charlson, R.L. Sani, On thermoconvective instability in a bounded cylindrical fluid layer, *International Journal of Heat and Mass Transfer* 14 (1971) 2157–2160.
- [21] R.J. Goldstein, K.-S. Lau, Laminar natural convection from a horizontal plate and the influence of plate-edge extensions, *Journal of Fluid Mechanics* 129 (1983) 55–75.
- [22] G.A. Ostroumov, Free convection under the conditions of the internal problem, S. Reiss (Trans.), Technical Report TM 1407, NACA, Washington, 1958 (Chapter 5).
- [23] C.-S. Yih, Thermal instability of viscous fluids, *Quarterly of Applied Mathematics* 17 (1959) 25–42.
- [24] K.E. Torrance, L. Orloff, J.A. Rockett, Experiments with natural convection in enclosures with localized heating from below, *Journal of Fluid Mechanics* 36 (1969) 21–31.
- [25] W.M. Lewandowski, P. Kubski, J.M. Khubeiz, Natural convection heat transfer from round horizontal plate, *Wärme- und Stoffübertragung* 27 (1992) 281–287.
- [26] R.A. Wooding, Instability of a viscous liquid of variable density in a vertical Hele–Shaw cell, *Journal of Fluid Mechanics* 7 (1960) 501–515.
- [27] W.M. Lewandowski, H. Bieszk, J. Cieśliński, Influence of cylindrical screens on free convection heat transfer from a horizontal plate, *International Journal of Heat and Fluid Flow* 12 (1991) 92–94.
- [28] D.K. Edwards, I. Catton, Prediction of heat transfer by natural convection in closed cylinders heated from below, *International Journal of Heat and Mass Transfer* 12 (1969) 23–30.
- [29] K.G.T. Hollands, Multi-Prandtl number correlation equations for natural convection in layers and enclosures, *International Journal of Heat and Mass Transfer* 27 (1984) 466–468.
- [30] J.D. Verhoeven, Experimental study of thermal convection in a vertical cylinder of mercury heated from below, *Physics of Fluids* 12 (1969) 1733–1740.
- [31] O.D. Kellogg, *Foundations of Potential Theory*, Dover, New York, 1953, p. 229.
- [32] Fluid Dynamics International. FIDAP 7.6 Update Manual. 500 Davis Street, Suite 600, Evanston, IL 60201, 1996.
- [33] E.M. Sparrow, G.A. Nunez, A.T. Prata, Analysis of evaporation in the presence of composition-induced natural convection, *International Journal of Heat and Mass Transfer* 28 (1985) 1451–1460.
- [34] G.A. Nuñez-Testa, Evaporation in the presence of isothermal and non-isothermal natural convection, Ph.D. thesis, University of Minnesota, Minneapolis, MN, 1986.
- [35] G.A. Nunez, E.M. Sparrow, Models and solutions for isothermal and non-isothermal evaporation from a partially filled tube, *International Journal of Heat and Mass Transfer* 31 (1988) 461–477.
- [36] E.M. Sparrow, G.A. Nunez, Experiments on isothermal and non-isothermal evaporation from partially filled, open-topped vertical tubes, *International Journal of Heat and Mass Transfer* 31 (1988) 1345–1355.
- [37] H. Suehrcke, J.A. Harris, Enhancement of water evaporation from a cylindrical container due to concentration induced free convection, in: R.W. Bilger (Ed.), *Proceedings of the Twelfth Australasian Fluid Mechanics Conference*, The University of Sydney, Sydney, Australia, 1995, pp. 891–895.
- [38] H. Suehrcke, J.A. Harris, G.D. McBain, Water evaporation from a cylindrical container: the Stefan problem revisited, in: S. Armfield (Ed.), *Fifth Australasian Natural Convection Workshop*, The University of Sydney, Sydney, Australia, 1996.
- [39] J.C. Buell, I. Catton, The effect of wall conduction on the stability of a fluid in a right circular cylinder heated from below, *ASME Journal of Heat Transfer* 105 (1983) 255–260.
- [40] H.G. Leopold, J. Johnston, The vapor pressure of the

- saturated aqueous solutions of certain salts, *Journal of the American Chemical Society* 49 (1927) 1974–1988.
- [41] J.L. Sohn, Evaluation of FIDAP on some classical laminar and turbulent benchmarks, *International Journal for Numerical Methods in Fluids* 8 (1988) 1469–1490.
- [42] G.D. McBain, Natural convection with unsaturated humid air in vertical cavities, *International Journal of Heat and Mass Transfer* 40 (1997) 3005–3012.
- [43] G.D. McBain, J.A. Harris, D.J. Close, H. Suehrcke, The effect of humidity on natural convection in vertical air filled cavities, in: E. Leonardi, C.V. Madhusudana (Eds.), *Proceedings of the Sixth Australasian Heat and Mass Transfer Conference*, Begell House, New York, 1998, pp. 49–56.
- [44] V. Haroutunian, M.S. Engelman, I. Hasbani, Segregated finite element algorithms for the numerical solution of large-scale incompressible flow problems, *International Journal for Numerical Methods in Fluids* 17 (1993) 323–348.
- [45] S.V. Patankar, *Numerical Heat Transfer and Fluid Flow*, Hemisphere, New York, 1980, p. 131.
- [46] Y. Jaluria, B. Gebhart, On the buoyancy-induced flow arising from a heated hemisphere, *International Journal of Heat and Mass Transfer* 18 (1975) 415–431.
- [47] C.J. Freitas, Editorial, *Journal of Fluids Engineering* 115 (1993) 339.
- [48] G.Z. Gershuni, E.M. Zhukhovitskii, *Convective Stability of Incompressible Fluids*, D. Louvish (Trans.), Keter, Jerusalem, 1976, p. 59.
- [49] J.M. Olson, F. Rosenberger, Convective instabilities in a closed vertical cylinder heated from below. Part I: monocomponent gases, *Journal of Fluid Mechanics* 92 (1979) 609–629.